Impact characterisation of low fibre-volume glass reinforced polyester circular laminated plates

L.S. Sutherland, C. Guedes Soares

Abstract

Drop-weight impact tests have been carried out for low fibre-volume glass-polyester laminates for a range of diameter to thickness ratios. Three damage stages were defined, 'un-delaminated', 'delaminated' and 'fibre damage'. Analysis of the impact response using a mainly graphical methodology allowed further characterisation of the behaviour. Impact damage occurs in two stages: hidden internal delamination damage at low incident energy, and then finally perforation failure. Bending and membrane effects are significant for thin laminates. For thick laminates shear deflection, delamination and indentation damage are more important. Some form of strain-rate stiffening effects appear to be significant for bending, but not for shear-controlled deflections or when damage is present. Indentation follows the Hertzian contact law at low contact forces, but a linear contact stiffness is seen at higher forces. A fracture mechanics model describes well the onset of delamination, and gives good scaling between specimen sizes. An energy balance approach gives good correlation between impact force and incident energy. Fibre failure leading to penetration is back-face tension controlled. The complex behaviour observed shows that the impact response must be characterised before mathematical modelling might be attempted. Modelling of the un-delaminated behaviour should consider bending, shear, indentation and membrane effects.

Keywords

Composite plates, Glass-polyester, Delamination, Fibre damage

Nomenclature

a_c : Contact area
A_o : Membrane stiffness constant
B_o : Bending stiffness constant
C_o : Shear stiffness constant
C_1 : Delaminated shear stiffness constant
E: Youngs modulus
G_{IIC} : Mode II strain energy release rate
h : Plate thickness
IKE : Incident kinetic energy
k : Contact stiffness
k_b : Bending stiffness
k_{bs} : Bending / shear stiffness
k_m : Membrane stiffness
k_s : Shear stiffness
P : Impact force

P_c : Critical delamination impact force

w : Plate deflection

w_c : Plate deflection at P_c

w_{Pmax} : Plate deflection at maximum P

α : Indentation

δ : Impacter displacement

ν : Poisson ratio

1. Introduction

The use of fibre reinforced plastic composite materials in a marine environment is advantageous mainly due to their ease of forming of double-curvatures, resistance to corrosion and rot, and high specific material properties. However, these materials are very susceptible to transverse impact damage both in terms of resistance and tolerance. In a marine environment, common impact events are collisions with other craft, docks, floating debris and grounding, all of which are low-velocity impacts. The normal production method in the marine industry is the hand lay-up of E-glass reinforcement with polyester resin. This gives notoriously variable quality, low fibre volume-fraction 'marine composites'.

Due to the interest in the potential weight-saving properties of composites for aerospace applications, a large amount of work has been published concerning high fibre volume-fraction, high quality, pre-impregnated, autoclave produced carbon-epoxy laminates. For the very few cases where glass fibre composites are studied these are of high fibre volume-fraction [1]. Impact data concerning 'marine composites' are scarce, and hence high safety factors and loss of potential weight savings are the norm. Mouritz et al. [2] quote safety factors of up to 10 applied when marine composite structures will be subjected to impact loads.

For an excellent overview of the impact of composites Abrate [3] provides a comprehensive review and classification of the field. For analysis purposes the impact event is usually split into two parts, localised contact and overall target deflection. Surface indentation is assumed to follow the Hertzian contact law [4,5]. Complete models may be used to exactly describe the deformation of the target using beam or plate theories or finite element modelling [6,7] for simple cases for small deflections and simple material architectures. However, these models are complex and will rapidly become very convoluted when more complex architectures, large deflections or cases with significant shear deformations must be considered. Significantly, they are not effective for the consideration of damage; in reality the response of a composite material to impact is complicated by numerous and interacting damage modes including internal delamination, surface micro buckling, fibre fracture and matrix degradation [8]. Damage mechanisms may vary with changes in the many material parameters such as fibre/resin type, ratio, architecture and interface, and laminate production method [9–11]. Hence, theories to describe the overall response, such as the energy balance and spring-mass methods [12] are more realistic.

Further, since these damage mechanisms are also highly dependent on the exact nature of the impact event [13,14] the impact response of a composite material has proved very difficult to standardise. Also, it is not clear which are the most relevant measures of impact

severity (e.g. incident energy, incident velocity, impact force) or even impact response (e.g. force, displacement, energy absorbed, impact duration). Recent work has attempted to further accommodate the complex damage mechanisms in terms of characterisation of the impact response [13] and through the use of combined theoretical-empirical models [15–18].

With respect to the complex impact behaviour Abrate [12] states that, "Sorting out these different types of behaviour is necessary for the interpretation of experimental results and the selection of an appropriate mathematical model." Here the aim is to provide a simple methodology to characterise the impact behaviour and thus to investigate the impact response of marine composites.

2. Experimental details

An orthotropic polyester resin (Aeropol FS 6902) was reinforced using a 500 gm^{-2} E-glass woven roving (Rovitex 500).1 m×1 m panels were laminated by hand on horizontal flat moulds to give a fibre mass-fraction of 0.5 (equivalent to a fibre volume fraction of approximately 0.35) as representative of the values commonly achieved under production conditions in the marine industry. 1%, 2% and 3% by mass of accelerator, catalyst and paraffin, respectively, were used, in an ambient temperature of between 18°C and 21°C, to cure the resin. Two sizes of specimens were cut from the panels using a diamond-surrounded circular saw. Panels of 3, 5, 10, and 15 plies were cut into 'small' 100 mm square specimens. Also, panels of 5, 10, 15 and 20 plies were cut into 'large' 200 mm square specimens. In order to ensure a full cure, all specimens were stored at room temperature for 4 months before testing. Thickness measurements were taken at four points on each specimen prior to testing.

Impact testing was performed using a fully instrumented Rosand IFW5 falling weight machine (Fig. 1). A small, light hemispherical ended cylindrical impacter is dropped from a known, variable height between guide rails onto a clamped horizontally supported plate target. A much larger, variable mass is attached to the impacter and a load cell between the two gives the variation of impact force with time. The data was filtered with a 2 kHz low pass filter to remove noise from the signal. An optical gate gives the incident velocity, and hence the impacter displacement and velocity and the energy it imparts are calculated from the force–time data by successive numerical integrations. Since the impacter is assumed to remain in contact with the specimen throughout the impact event, the impacter displacement is used to give the displacement and velocity of the top face of the specimen, under the impacter. By assuming that frictional and heating effects are negligible, the energy imparted by the indenter is that absorbed by the specimen. Thus, this energy value at the end of the test is that irreversibly absorbed by the specimen.

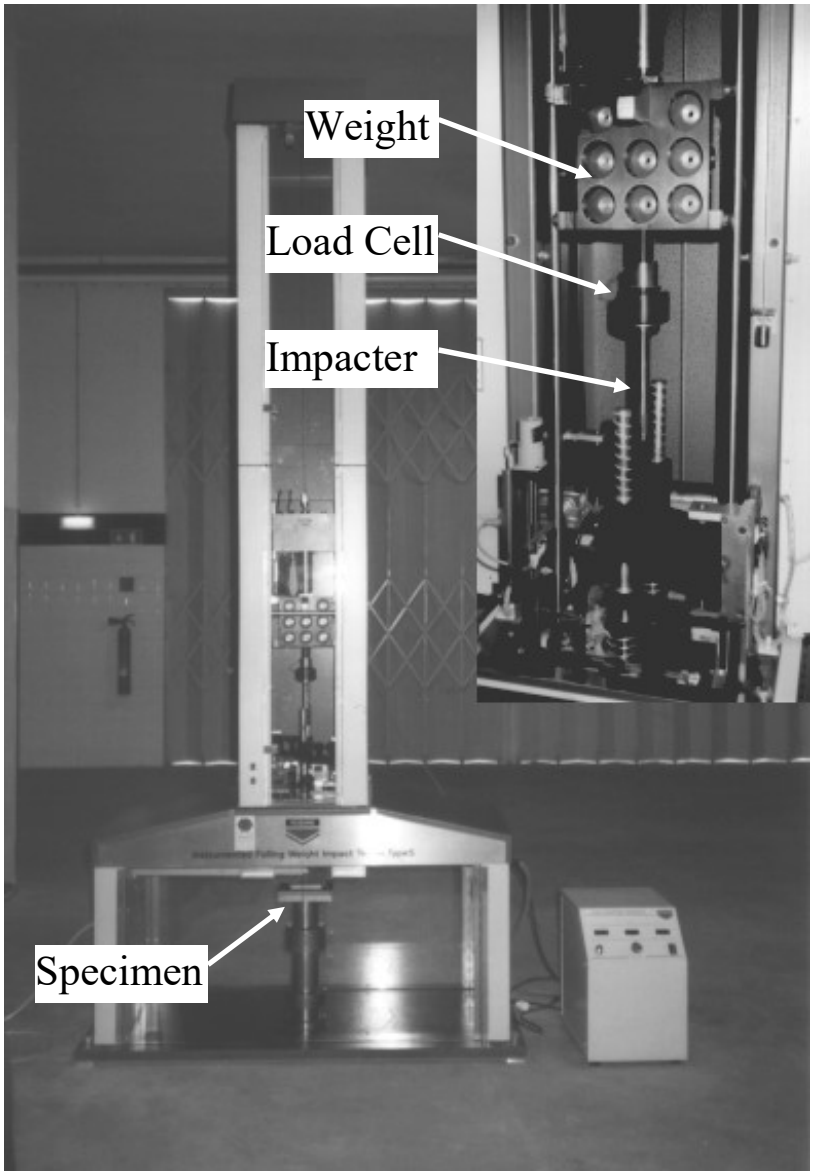

Fig. 1. Impact machine.

The specimens were fully clamped between two thick annular circular steel plates. The clamping force was applied using a pneumatic actuator and a long lever arm to achieve high forces. The 'small' and 'large' specimens were tested using clamps with inside diameters of 50 and 100 mm, respectively. A 10 and 20 mm diameter impacter were used to strike the small and large specimens, respectively.

Tests were performed for a range of increasing incident energies either up to perforation where possible, or to the maximum attainable by the machine. Nominally the impact masses used were 2.853 and 10.853 kg for the small and large specimens, respectively. Impact velocities of between 0.37 and 6.19 ms^{-1} were achievable using the machine. The mass used for some of the higher incident energy impacts of the small specimens was increased to give perforation: The masses for the 10-ply 75, 95 and 110 J tests were 3.85, 4.85 and 5.85 kg, respectively, and for the 15-ply 60, 80, 100, 130, 150 and 170J tests 3.85, 4.85, 5.85, 6.85, 7.85 and 9.85 kg, respectively, were used.

After testing, the various types of damage were observed and noted. Since the material is translucent, the projected internal delamination area, where present and approximately circular, could be measured using strong backlighting.

3. Results

The impact behaviour seen was complex, but followed general trends as will be described here together with illustrative examples. Since the nature of these trends varied somewhat with specimen thickness it is instructive to consider the values given in Table 1. It is of note that the thickness variability decreases with increasing number of plies. This is thought to be because most of the variation in thickness is due to the uneven nature of the surface ply, and that this variation remains approximately constant with thickness. In terms of thickness to diameter ratio the small 5- and 10-ply specimens are equivalent to the large 10- and 20-ply specimens, respectively.

Clamp	Number of Plies	Thickness (mm)	Coefficient of Variation	Diameter / Thickness
Small 50mm	3	1.94	0.10	26
	5	3.31	0.04	15
	10	6.58	0.05	8
	15	9.80	0.04	5
Large 100mm	5	3.28	0.07	30
	10	6.49	0.07	15
	15	9.15	0.04	11
	20	12.41	0.03	8

Table 1. Specimen thickness

A number of tests at the highest incident energies were repeated with the pneumatic clamping system replaced with bolts that passed through the clamps and the clamped edges of the specimens. These results showed conclusively that the pneumatic system provided sufficient force to clamp the specimens.

3.1. Damage modes

Some form of damage was observed at all but the very lowest incident energies. The many different damage modes seen were: matrix cracking, matrix degradation, permanent indentation, internal delamination, partial surface micro-buckling delamination of the upper ‘front-face’ laminate, front-face fibre damage, fibre damage on the lower ‘back-face’, and perforation. These modes form a complex overall damage pattern, but the progression of damage with increasing incident energy is similar for all specimens and all of the main features may be described by broadly categorising the damage progression into that for thin and thick specimens as described below. ‘Thin’ and ‘thick’ in this case may be loosely defined as those with diameter to thickness ratios of greater than and less than 15, respectively.

Thin specimens:

(i) At the very lowest incident energies obtainable (1 or 2 J) no damage is visible. The first signs of damage are matrix cracks, internally or at the back face, which follow the woven pattern of the rovings.

(ii) Still at a very low incident energy a roughly circular, central, internal delamination occurs, which also follows the woven pattern of the rovings. Delamination occurs at more than one ply interface. Delaminated zones form on the front-face at the points where one roving passes over another. A small permanent indentation occurs under the impacter.

(iii) The delamination areas increase gradually. Back face matrix damage is seen. Concentric rings of front-face matrix cracks close to the clamp edges occur.

(iv) Back-face fibre damage occurs. This is swiftly followed by front-face fibre damage, which leads to the start of perforation. Perforation develops until full penetration of the specimen is achieved.

Fig. 2 shows three panels from the small 3-ply tests as an illustration of the failure modes seen for the thinner laminates. The left-, middle- and right-hand specimens correspond to (ii), (iii) and (iv) above, respectively.

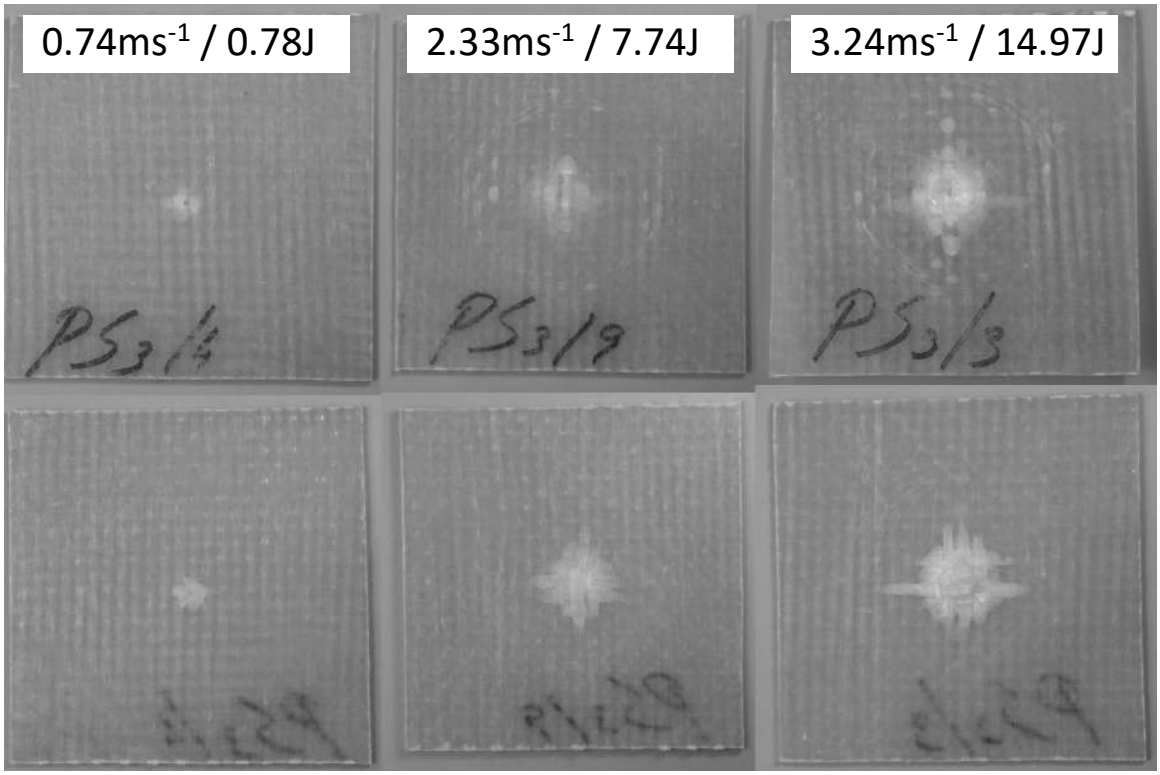

Fig. 2. Impacted thin laminates (3-ply 50 mm diameter, front-face top row, and back-face bottom row).

Thick specimens:

(i) At the very lowest incident energies obtainable (2 J) only an extremely small local circular front-face delamination under the impacter is seen. As with the thin specimens, matrix cracks, which follow the woven pattern of the rovings, appear internally or at the back face.

(ii) Also as for the thin specimens, at a low-incident energy a circular, central, internal delamination suddenly occurs. Delamination again occurs at more than one ply interface, but is largest closer to the back-face. An area of delaminated zones forms on the front-face at the roving 'cross-over' points, which is small in comparison to the internal delamination. A small permanent indentation occurs under the impacter.

(iii) The internal and front-face delamination areas increase rapidly, whilst the permanent indentation becomes more severe. Next, the front-face delamination with matrix damage becomes pronounced in a central cross-shaped area that follows the weave directions, and internal delaminations become irregular in shape.

(iv) At around the same incident energy that the delamination reaches the clamp edges, the front-face fibres under the impacter sustained damage. Where sufficiently high incident energies were attainable, this fibre damage became partial and then full perforation.

Fig. 3 shows three panels from the large 20-ply tests as an illustration of the failure modes seen for the thicker laminates. The left-, middle- and right-hand specimens correspond to (i), (ii) and (iii)/(iv) above, respectively.

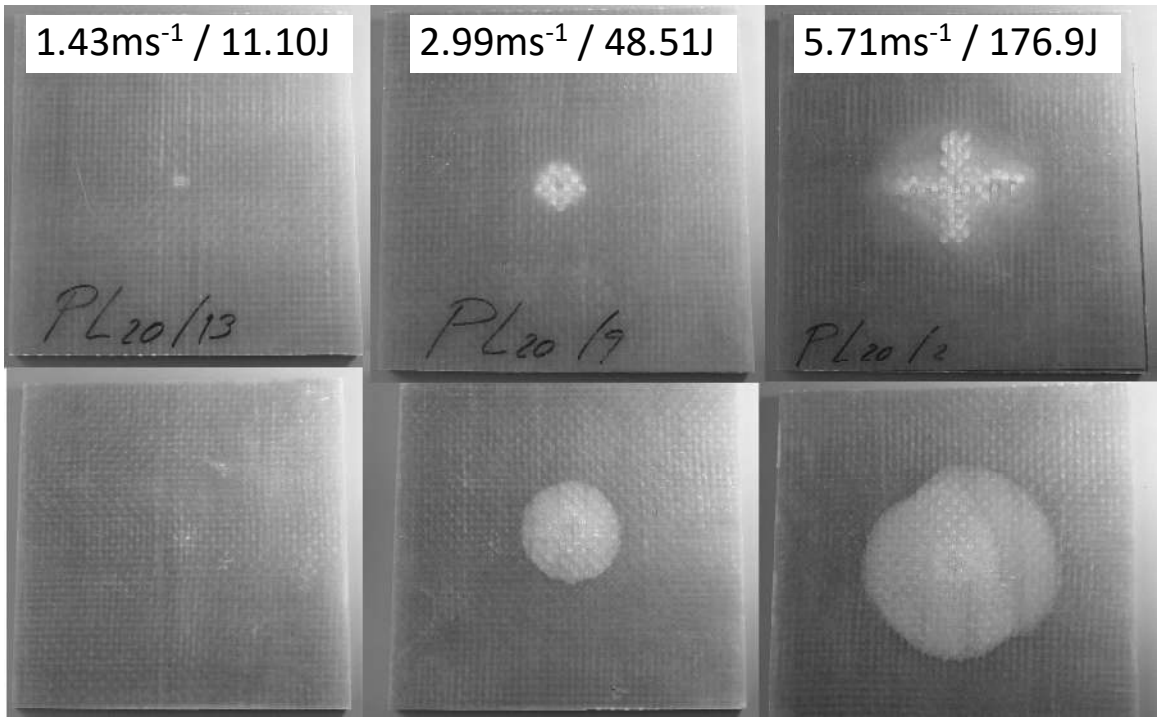

Fig. 3. Impacted thick laminates (20-ply 100 mm diameter, front-face top row, and back-face bottom row).

The descriptions above show that, although subtly different, both thick and thin specimens exhibit the same three main stages of damage progression. Hence, it is helpful to characterise the damage behaviour with three separate 'regimes':

1. *'Un-delaminated'*: At extremely low incident energies damage is slight and mainly restricted to matrix cracking.

2. *'Delaminated'*: At a low critical incident energy delaminations suddenly appear, which then spread with increasing impact severity.
3. *'Fibre damage'*: At higher energies fibre failure occurs, leading to perforation.

Importantly, since the damage seen is directly responsible for the behaviour seen, these definitions also allow simple characterisation of the impact response. In all graphs that follow, points containing a cross indicate no delamination and those containing a dot indicate observed fibre failure (either front and/or back face).

3.2. Force–displacement and force–time response

Force–displacement and force–time plots present the raw experimental data in a simple and easily interpreted form. The data for the thinnest (3-ply small) and thickest (20-ply large) specimens are shown in Figs. 4 and 5, respectively. Each shows a family of curves for increasing incident energy.

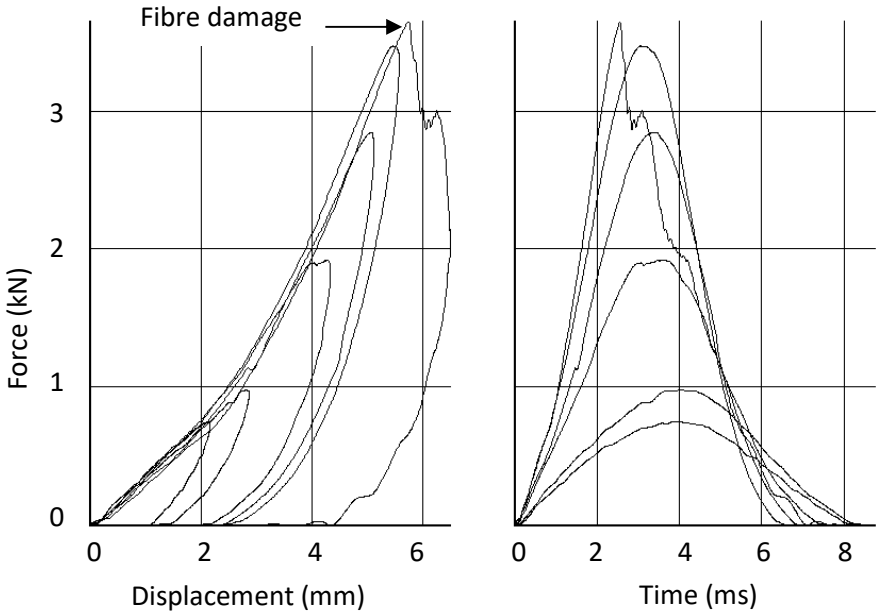

Fig. 4. Impact response thin laminate.

First consider the thin laminate behaviour in Fig. 4. The main feature is the increasing stiffness with displacement due to large deflections and the associated non-linear membrane effects. For the lowest energies both curves are smooth and the force–time response approximately symmetric, indicating no severe damage. However, the area under the force–displacement curves indicate considerable incident energy is irreversibly absorbed by the laminate even at these low energies (see Section 3.3). The onset of delamination is not reflected in the force–displacement plot, but some evidence of this damage may be seen in force–time response, although this remains approximately symmetrical right up to the onset of fibre failure. At high incident energy the effect of fibre damage is evident as a sharp drop in force with both displacement and time and a highly asymmetric force–time response.

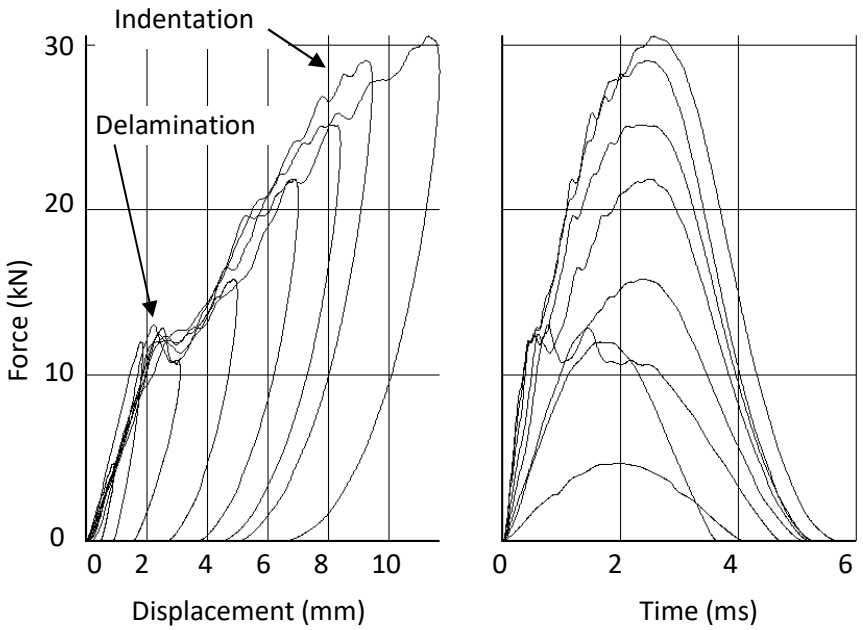

Fig. 5. Impact response thick laminate.

Next, consider the case of the thick laminate in Fig. 5. The obvious feature here is the bi-linear nature of the force–displacement plot, due to a sudden drop in stiffness as delamination occurs. The response of the lowest energy impacts is as in Fig. 4, but the onset of delamination is clear here in both the force–displacement curves and in the highly asymmetric force–time curves. Although this delamination was seen to grow with incident energy, the delaminated stiffness remains approximately constant. The observed indentation damage is reflected in the jagged form of the curves at higher forces. Although the test machine could not achieve the energy required to perforate these thick specimens, at the highest energy in Fig. 5 the effects of the beginnings of this process can be seen.

The forms of the curves indicate that it would not be necessary to carry out such a large number of tests to characterise the force–displacement impact response. For the thin specimens a small number of tests at a high incident energy would suffice, and for the thicker specimens this would be then complimented well by tests around the delamination incident energy.

3.3. Irreversibly absorbed energy

The energy irreversibly absorbed by the small and large specimens is presented in Figs. 6 and 7, respectively. Approximately 75% of the incident energy is irreversibly absorbed until fibre damage absorbs more energy. Hence, even at the lowest incident energies the laminate absorb a significant amount of the incident energy, although no delamination has occurred, as mentioned in Section 3.2. Whether this is due to hidden damage such as matrix micro-cracking, or due to other mechanisms such as friction or visco-elastic effects is not clear and requires further investigation. In both graphs for thicker specimens at higher incident energies, the points rise above the line before a dot indicates the presence of fibre damage. This is thought to indicate the energy absorbing effect of increased indentation damage. These plots do not indicate the onset of delamination.

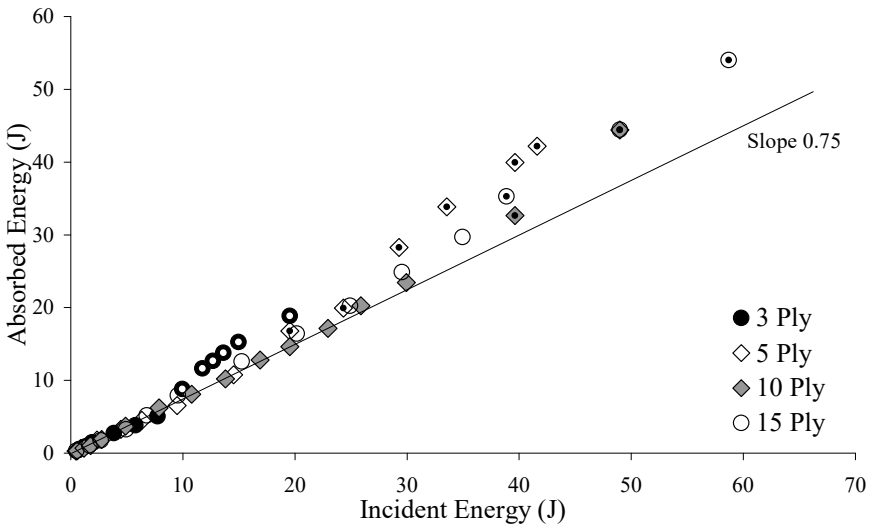

Fig. 6. Irreversibly absorbed energy, 50 mm diameter specimens.

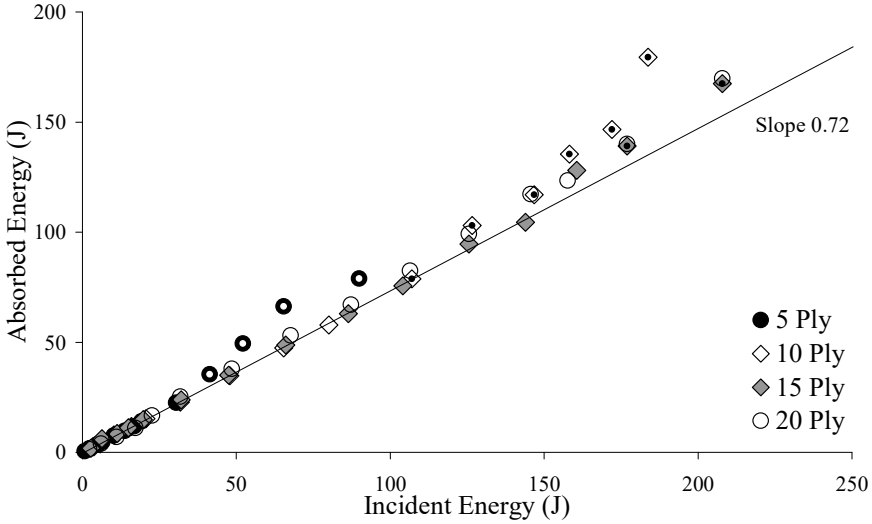

Fig. 7. Irreversibly absorbed energy, 100 mm diameter specimens.

3.4. Impact duration

Figs. 8 and 9 show the durations of the impacts of the small and large specimens, respectively. For an undamaged, non strain-rate dependant material the impact duration will be independent of incident energy and will decrease with increasing stiffness. Damage will extend the impact event. Here, two distinct types of behaviour are seen.

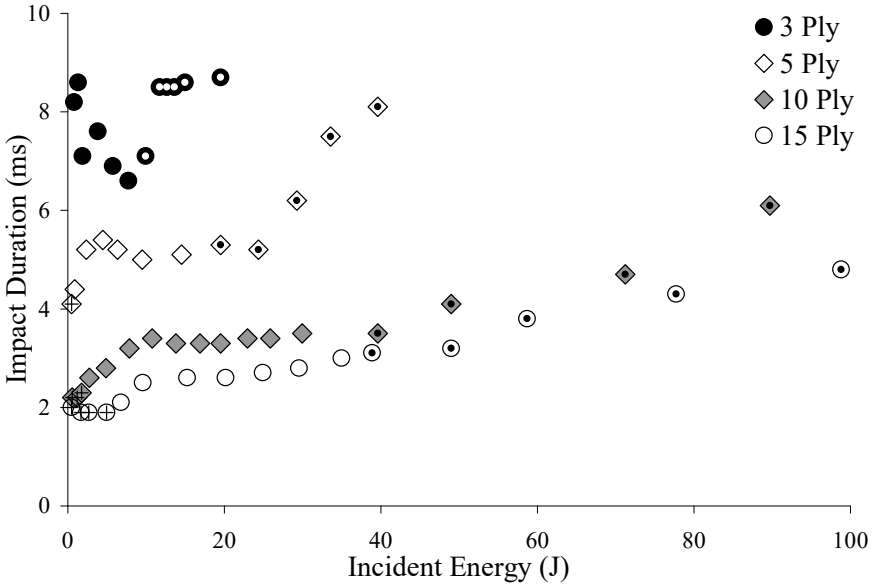

Fig. 8. Impact durations, 50 mm diameter specimens.

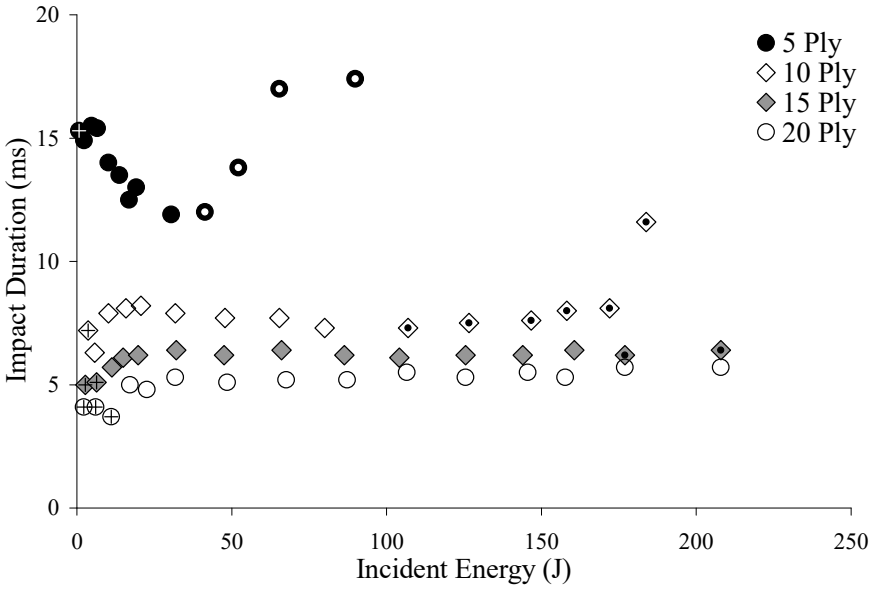

Fig. 9. Impact durations, 100 mm diameter specimens.

The thinnest specimens, small 3-ply and large 5-ply, show a marked decrease in duration with increasing incident energy, until this once again rises with the onset of fibre damage. This is despite the fact that delamination damage is present for all but the lowest energy large 5-ply test. Here the stain rate increases with greater incident energy since the duration is nominally constant whilst displacement increases, indicating that rate-dependant material properties could be important. 'Strain-rate effects' increasing failure load and stiffness of glass fibre composites have been reported [1,19], typically concerning increases in strain-rate of more than one order of magnitude or comparing static with impact tests. However, strain-rate increases of only approximately three- and five-fold for the small 3-ply and large 5-ply specimens, respectively, are seen here. Also, the increase in stiffness that would be associated with this decrease in duration is not immediately evident in Fig. 4. Visco-elastic effects due to the high proportion of resin could also be important here, as could interactions between strain rate and the delamination propagation rate.

The other thicker laminates show no such reduction in duration, for the un-delaminated regime duration remains constant. This duration increases as delamination occurs, and then remains relatively constant until fibre damage again prolongs the impact event. For the thickest laminates impact duration increases slightly before fibre damage due to indentation damage. The intermediate, small 5-ply and large 10-ply specimens show a slight shortening of impact duration after delamination.

This difference in behaviour is thought to be because, as will be discussed in Section 4.2, bending controls the response of the thinnest laminates whereas for the thicker specimens shear and indentation dominate, perhaps indicating why effects of strain-rate are not always seen to be significant [17]. Clearly this complex question of strain-rate dependant behaviour requires further investigation.

4. Analysis and discussion

An inspection of the results presented in the form of force–displacement, force–time, irreversibly absorbed energy and impact duration has enabled the complex impact behaviour to be correlated with the various physical processes occurring. Now, a simplified theoretical analysis of the system will aim to extend this methodology for the characterisation of the impact response.

The geometry of the impact event is defined in Fig. 10. The measured *displacement* of the impacter (δ) is made up of the sum of the plate *deflection* (w) and the *indentation* (α).

i.e. $$\delta = w + \alpha \qquad (1)$$

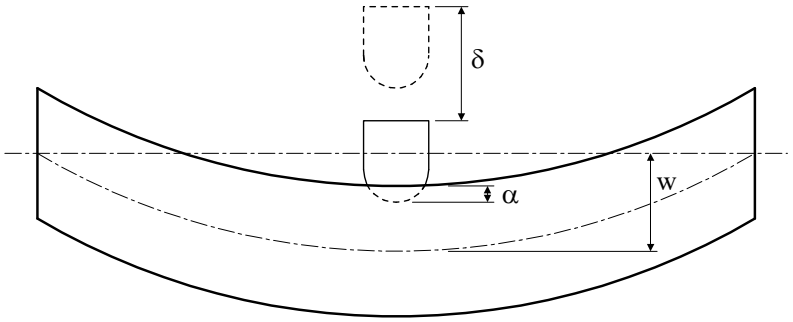

Fig. 10. Impact geometry.

4.1. Indentation

Contact force P is related to the indentation by the Hertzian contact law. For a rigid spherical indenter and a transversely isotropic half-space this may be expressed as [5]:

$$P = k\alpha^{3/2} \qquad (2)$$

where k is a contact coefficient depending on target and sphere material properties and the sphere radius.

Since these WR composites are only approximately transversely isotropic and the surface is not flat, quasi-static tests were carried out to confirm this contact law. 30-ply specimens were laminated according to the method in Section 2 and supported on a thick flat steel

base. The same 10 and 20 mm diameter hemispherical ended cylinders as used for the impact tests were pushed down onto specimens at speeds of 0.2 and 0.3 mm/s, respectively. Only one 10 mm test was successful, but since the repeatability of the six 20 mm tests carried out was extremely high, this was assumed to be acceptable. The results (average values for the 20 mm tests) are shown in Figs. 11 and 12.

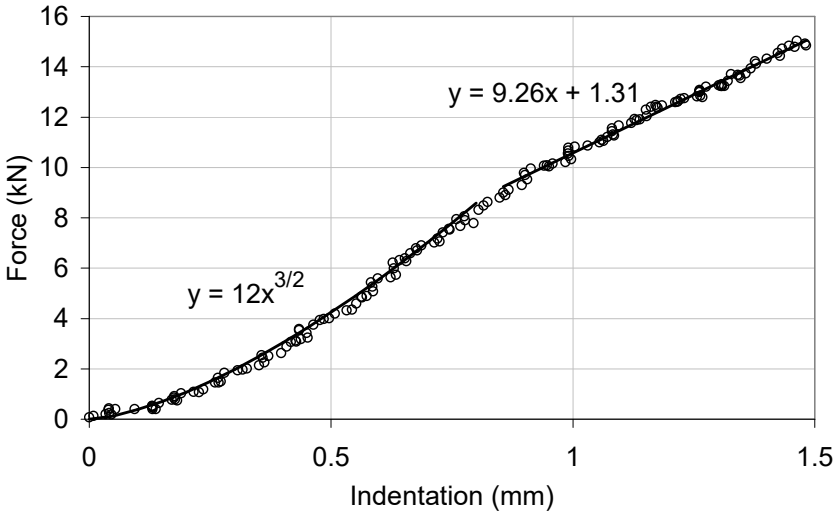

Fig. 11. Indentation test results for 10 mm diameter indenter.

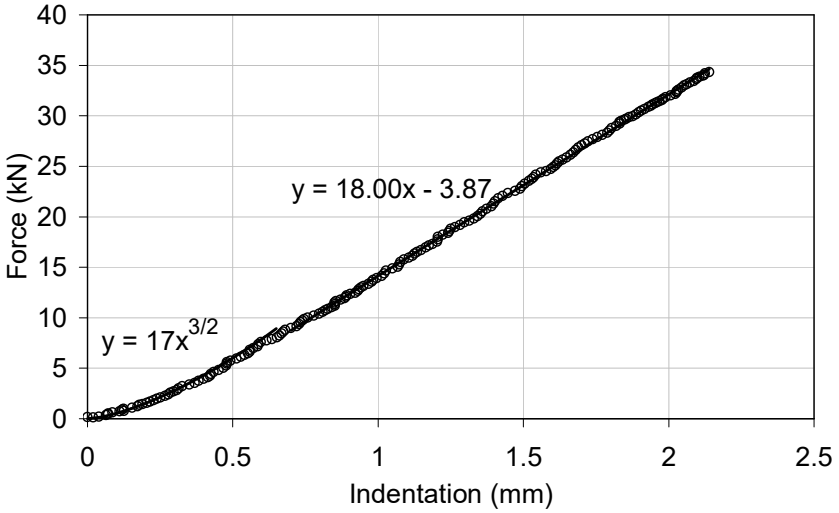

Fig. 12. Indentation test results for 20 mm diameter indenter.

Up to a force of around 9 kN both graphs show that Eq. (2) describes very well the indentation stiffness. Moreover, k is 1.2 and 1.7 kN mm$^{-3/2}$ for the 10 and 20 mm diameter tests, respectively. This agrees extremely well with the expectation that k is proportional to the square root of indenter diameter [12,20].

However, between 9 and 10 kN the data start to deviate considerably from Hertzian behaviour. At higher loads a very linear relationship exists between force and indentation. Current work by the authors indicates that even at lower loads when the Hertz law is applicable permanent indentation occurs. However, at higher loads damage becomes much more severe, consisting of matrix degradation, delamination and then fibre damage, and leads to the linear behaviour seen.

It should be noted here that the geometry of the impact tests differs slightly from that of the indentation tests. For the impact tests progressive bending of the specimens leads to a greater contact area. Some researchers [5] have allowed for this by measuring the indenter movement and that of the back face. Here this approach was not thought to be advantageous for the following reasons: this effect is most prominent in the thinner specimens where bulging of the back face will make the method inaccurate; indentation is most significant for the stiffer and thicker specimens where the geometry is close to that of the indentation tests. The measurement of such small displacements leads to accuracy problems which will be greatly increased by the measurement of the back-face movement relative to that of the indenter. Also the unevenness of the surface probably introduces much greater deviations from the geometry, making such effects insignificant. Hence, the indentation results will be used with Eq. (1) to give the plate deflections, *w*, to be considered in the next section.

4.2. Plate deflection

The simplest plate-bending problem assumes a thin plate with small deflections [21]. However, here the behaviour is much more complex, including both large deflections of thin plates where membrane effects become important, and also deflection of thick plates where the effects of shear must be considered.

Shivakumar et al. [20] provide the relationship between impact force *P* and plate deflection *w* in terms of bending, shear and membrane stiffness (K_b, K_s and K_m, respectively) for a centrally loaded circular plate:

$$P = K_{bs} w + K_m w^3 \quad (3)$$

$$K_{bs} = \frac{K_b K_s}{K_b + K_s} \quad (4)$$

Expressions for the stiffness are also given for the four permutations of clamped or simply supported specimens with immovable or movable edges. These are of the form:

$$K_m = A_o h; \quad K_b = B_o h^3; \quad K_s = C_o h \quad (5)$$

where *h* is laminate thickness, A_0, B_0 and C_0 are constant for a given material and plate diameter, and in the case of C_0, assuming the contact area a_c is constant.

Here the aim is to characterise the complex behaviour seen. Based on the behaviour seen in previous work [22] some gross assumptions about the response will be made and then deviations of the data from simple representations of the simplified model will be used to distinguish various types of behaviour.

The first simplification is that shear and bending dominate the behaviour and that membrane effects are negligible. Hence, assuming K_m is zero and combining Eqs. (3)–(5) gives:

$$\frac{P}{h} = C_o \left(\frac{h^2}{h^2 + C_o / B_o} \right) w \qquad (6)$$

Hence, a simple plot of impact force normalised with thickness against plate deflection should yield a straight line for a given laminate thickness, material properties and plate diameter. This line should increase in slope as the number of plies increases, asymptotically approaching a limiting value for thick laminates. For these thicker laminates shear deflections dominate and Eq. (6) may be further simplified to give:

$$\frac{P}{h} = C_o w \qquad (7)$$

Of course, the laminate thickness at which shear deflections dominate depends upon the term C_0/B_0, which is dependent upon the material properties and the specimen diameter. If shear deflections dominate then the simple plot of impact force normalised with thickness against plate deflection should yield a straight line with a slope that is independent of the number of plies. In Figs. 13 and 14 the maximum force normalised by thickness is plotted against the corresponding plate deflection for each test. Again points containing a cross indicate no delamination and those containing a dot indicate fibre failure.

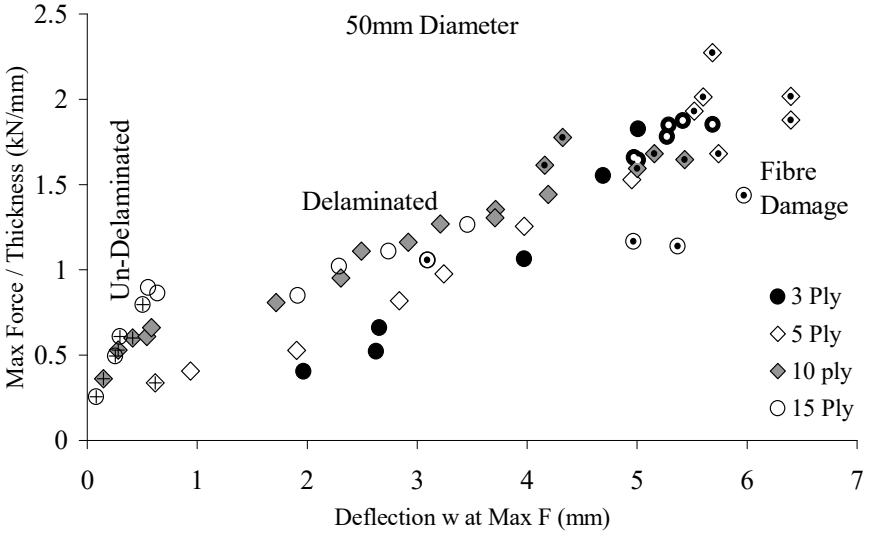

Fig. 13. Small specimens, maximum force.

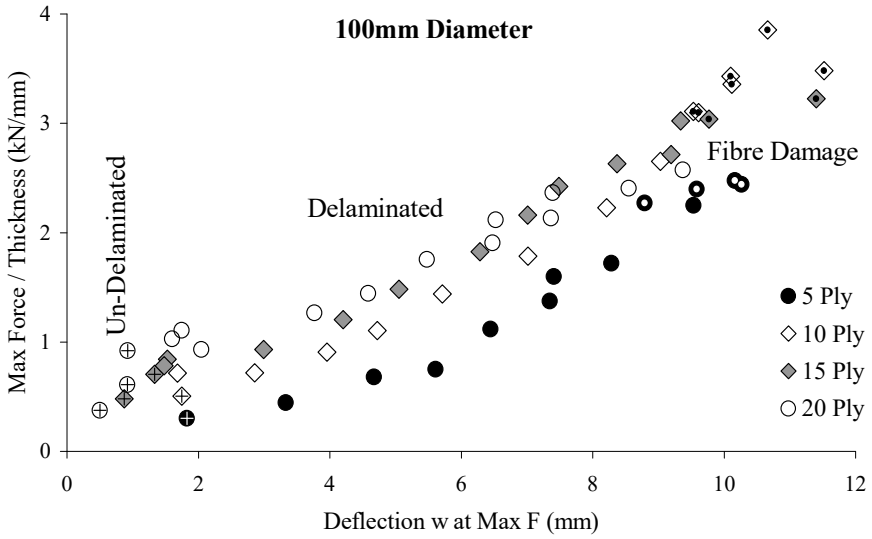

Fig. 14. Large specimens, maximum force.

The overall trend of both graphs is that of an initial, stiffer, linear un-delaminated response, followed by a less stiff delaminated response. However, there are various variations in the basic behaviour and these various responses and the damage mechanisms responsible for them may be identified from these simple plots. The behaviour may again be categorised into that of thin and thick specimens (again, in terms of diameter to thickness ratio), with the small 5-ply and large 10-ply specimens lying somewhere between the two.

Let us first consider the thicker specimens. The behaviour at low deflections and loads is linear with a 'thickness-normalised stiffness' that appears to be approaching a limiting value for the thickest laminates. This indicates that the response has a significant shear effect even for these un-delaminated specimens. A sudden drop in the maximum force marks the sudden onset of delamination. This occurs at a low incident energy and is further discussed in Section 4.3. The delaminated response is linear with a reduced normalised stiffness independent of thickness indicating shear-dominated behaviour.

The thinner specimens exhibit a slightly different behaviour. The reduction of the lower normalised stiffness with decreasing thickness indicates that bending is dominant. Although few data points are available at very low forces, the first large 5-ply point of Fig. 14 and the force–displacement plots of Fig. 4 indicate that an initial short-lived linear response is present. The thinnest laminates show no significant effect of the onset of delamination, but the upward-curving response at higher deflections shows that the effects of in-plane membrane forces become important until fibre damage occurs.

For the small 3- and 5-ply laminates at higher deflection (and hence incident energies), the maximum load tends to level off as perforation becomes pronounced. The available incident energy was not sufficient to give full perforation of the small 10-ply and the large 5-, 10- and 15-ply laminates and hence in these cases similer behaviour was not reached although fibre damage was observed. For the thickness specimens (small 15-ply and large 20-ply) the increase in force with deflection is also curtailed at higher deflections. In this case it is thought that this is due to indentation damage leading to perforation. The large 20-ply specimens show considerable indentation damage without full perforation, and a sligh levelling off of the force at displacement of between 7 and 9 mm before fibre damage occurs reflects this. The onset of fibre damage is further discussed in Section 4.5.

4.3. Delamination

Since the delamination has been seen to be the first significant damage leading to a reduction in material properties it is important to be able to predict its onset. This is especially important since even for this opaque material, pigmented gelcoat or paint will mean that delamination damage will be hidden for in-service laminates. Such damage may lead to a local stiffness reduction, and possible damage growth with cyclic loading and/or water ingress leading to a later loss of the vessel or its value. Since delamination occurs at such low incident energies it must be asked how many vessels have considerable undetected delaminations due to minor, everyday impacts?

Davies et al. [1,23,24] use a simple mode II fracture analysis to describe the critical load for the unstable onset of a single circular delaminating in an isotropic material:

$$P_c = \frac{2\sqrt{2}\pi}{3}\left(\frac{EG_{IIc}}{1-\nu^2}\right)^{1/2} h^{3/2} \qquad (8)$$

where E is Young's modulus, G_{IIc} is the mode II strain energy release rate, ν is Poisson's ratio, and h is laminate thickness.

Davies et al. used this approach fairly successfully for carbon epoxy [23], but did not obtain satisfactory results for high fibre-volume fraction glass polyester laminates [1]. Cartié and Irving [9] obtained such good correlation using this method for CFRP that they advocated the use of impact testing to determine G_{IIc}. Christoforou [13] also used Eq. (8) to define the onset of delamination.
A logarithmic plot of P_c against h for the tests carried out here is drawn in Fig. 15. The theory fits the data extremely well, as shown by the R^2 value of 99.9%, although the slope is slightly higher than the theoretical value of 1.5. Importantly, the theory scales extremely well between the small and large specimens.

From the intercept, taking Young's modulus as 13 MPa (from four-point bending tests) and assuming ν=0.3, G_{IIc} can be estimated to be 1.0 N/mm. In the literature G_{IIc} data is scarce, and was not found for the material observed here. However, Hancox and Mayer [19] quote a G_{IIc} value of 1.2 N/mm for E-glass epoxy and Zhou and Davies [1] give a value of 4.2 N/mm for high volume fraction E-glass polyester. Although for different materials, considering the difficulties in measuring $G_{IIc,}$ and the lack of a standardised method [9], the fact that these values are close to that obtained here, together with the goodness of fit, instills confidence in the theory.

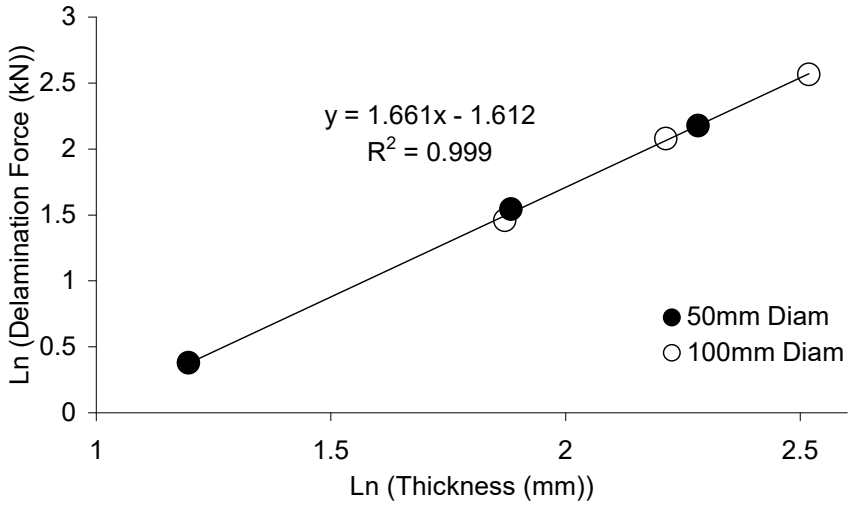

Fig. 15. Critical delamination force vs. laminate thickness.

4.4. Energy balance

The next logical step is to characterise the relationship between the severity of the impact event and the force-deflection behaviour. Here, in consideration of the complexity of the damage paths present, an energy balance approach is taken. It is assumed that at the maximum force the specimen has absorbed all the incident energy. This is valid since maximum force and maximum deflection occur very nearly simultaneously for all tests where fibre damage is not significant.

Calculating the energy absorbed by integration of the force-deflection response and normalising both sides by thickness gives:

$$\frac{IKE}{h} = \int_0^{w_{P,Max}} \frac{P}{h}\,dw \qquad (9)$$

Again, since the object is to characterise the behaviour, the gross assumption that shear deflections are dominant is made and then deviations from this behaviour are used to identify the different mechanisms. Since in Section 4.2 the force-deflection behaviour for thicker specimens was bi-linear (Fig. 5), Eq. (7) may be modified accordingly:

$$\frac{P}{h} = C_0 w \quad (a) \qquad \text{and} \qquad \frac{P}{h} = C_1 w + (C_0 - C_1) w_C \quad (b) \qquad (10)$$

$$\text{for } w \le w_C \qquad\qquad \text{for } w \ge w_C$$

where C_0 and C_1 are the "thickness-normalised stiffness'' of the un-delaminated and delaminated behaviour and w_C is the deflection corresponding to P_c.

Substituting for P/h from Eq. (10) into Eq. (9) and integrating gives:

$$\frac{IKE}{h} = \frac{1}{2}\left(C_1 w_{PMax}^2 + 2(C_o - C_1) w_C w_{PMax} + (C_1 - C_o) w_C^2\right) \quad (11)$$

Using Eq. (10) to express this result in terms of maximum force gives:

$$\left(\frac{P_{Max}}{h}\right)^2 = 2C_o\left(\frac{IKE}{h}\right) \qquad (a)\ for\ P \le P_C$$

$$\left(\frac{P_{Max}}{h}\right)^2 = 2C_1\left(\frac{IKE}{h}\right) + \left(\frac{C_o - C_1}{C_o}\right)\left(\frac{P_C}{h}\right)^2 \qquad (b)\ for\ P \ge P_C \quad (12)$$

Hence, plots of $(P_{max}/h)^2$ against IKE/h should also be of a bi-linear form, and the data is plotted accordingly in Figs. 16 and 17. In both graphs the un-delaminated behaviour forms only a small part of the response, where as expected the variation of slope with thickness is as discussed in Section 4.2. The limiting of maximum force due to fibre damage at high incident energies is also evident. The upward-curving trend of the thinner laminates due to membrane effects and the slight reduction in maximum force before fibre damage due to indentation damage for the thickest laminates are also again evident.

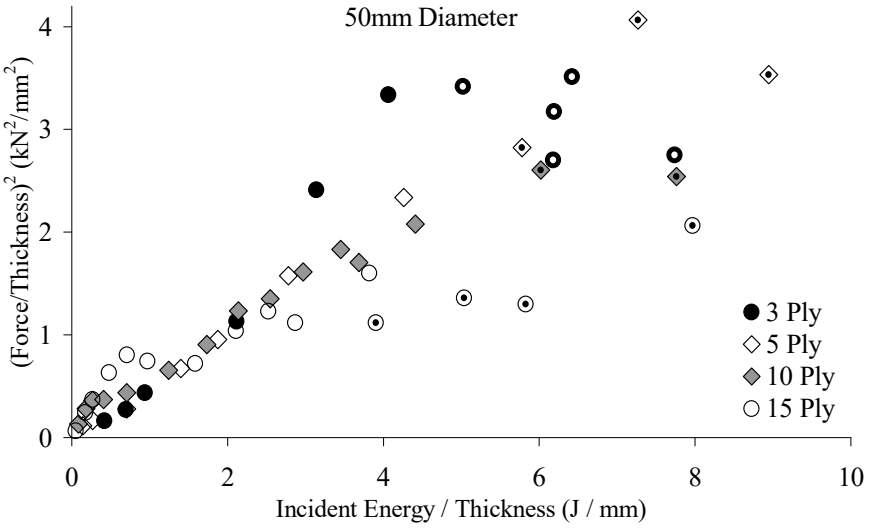

Fig. 16. Small specimens, energy balance plot.

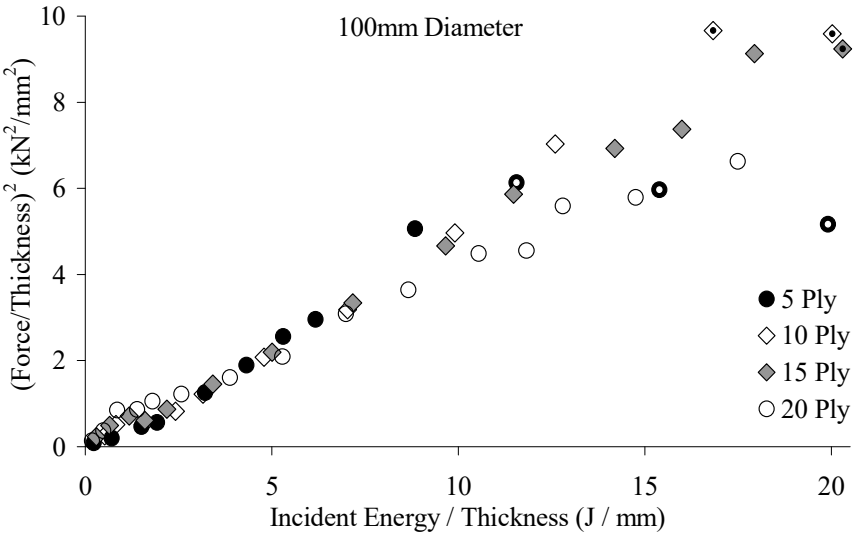

Fig. 17. Large specimens, energy balance plot.

However, the most important point is that the data collapses very well onto a linear trend for the delaminated response. This linearity is seen for the bulk of the incident energy range and is of a very similar slope in both graphs. Eq. (12b) predicts that, for shear dominated behaviour, the delaminated response should consist of a series of parallel lines with those for thicker laminates lying above those for thinner laminates (see broken lines in Fig. 18) due to the increase in the critical delamination load P_c with thickness as seen in Section 4.3. However, in Figs. 16 and 17 this is not the case; after delamination all data collapse onto the same linear trend. This is because Eq. (10b) and hence Eq. (12b) does not consider the initial sudden growth of the central delamination and the associated unstable increase in deflection at constant load (see Fig. 5). This effect of this unstable delamination is to shift the delaminated data points to the right in Figs. 16 and 17 as shown schematically by the solid lines in Fig. 18. Here, for each laminate thickness the effect of the initial unstable delamination is almost exactly offset by that of the increase in P_c with thickness, and the delaminated data points lie on the same linear trend independent of laminate thickness. It is not clear from the present work if there is a physical basis for this almost exact negation of effects, or whether this is merely a coincidence for the current test set-up. However, this behaviour is seen for both small and large specimens and even the data for the thinnest specimens where bending is significant follow approximately the same linear trend until membrane effects become dominant.

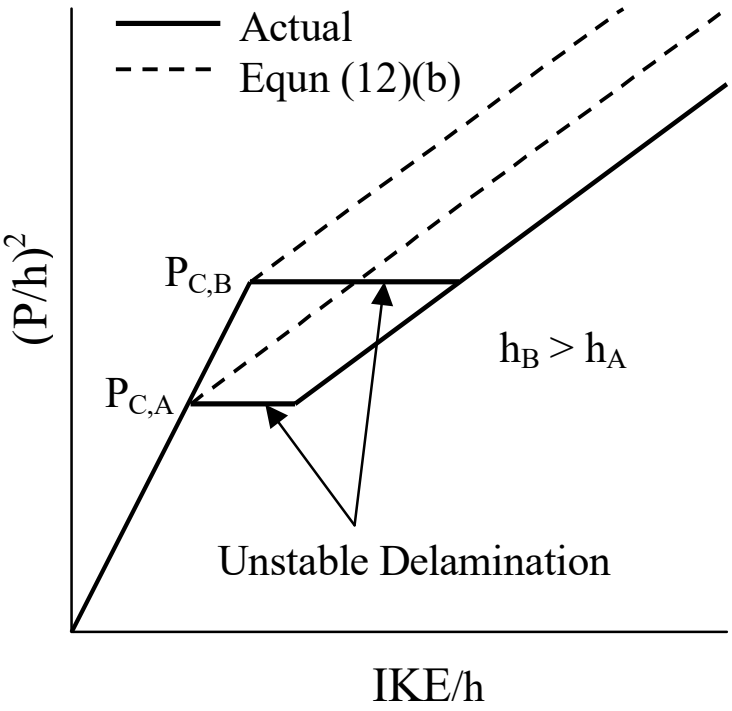

Fig. 18. Effect of unstable initial growth of internal delamination.

4.5. Fibre failure

The onset of significant fibre damage is clear from the jagged form of the load-displacement plot such as Fig. 4. Here, in order to further understand the nature of fibre damage and the ensuing perforation, an attempt to quantify this visual method will be made. For the highest IKE test in Fig. 4 the displacement increases, as fibres are broken, after the maximum load has been reached. That is, the maximum load and displacements no longer occur simultaneously. Hence, a pertinent indicator of fibre damage is the difference between the maximum displacement and the displacement at maximum force.

It is thought that fibre damage leads to perforation, but there are two possible damage paths that could lead to perforation: (i) Excessive bending causes back-face fibre tensile failure, and (ii) Excessive contact force that causes front-face fibre 'shear-out' failure. It is logical to assume that if (i) were controlling then fibre failure should occur at a critical plate deflection for a given plate diameter. Conversely, if (ii) were controlling then fibre failure should occur at a critical contact force, independent of plate diameter. In fact, the former case of back-face tensile fibre failure is shown to be controlling as shown in Figs. 19 and 20. Fibre damage leading to perforation may lead to a direct loss of the vessel. The perforation mechanism seen explains why high strain to failure fibres such as Kevlar are recommended for impact resistance. The onset of delamination is also discernable in these plots.

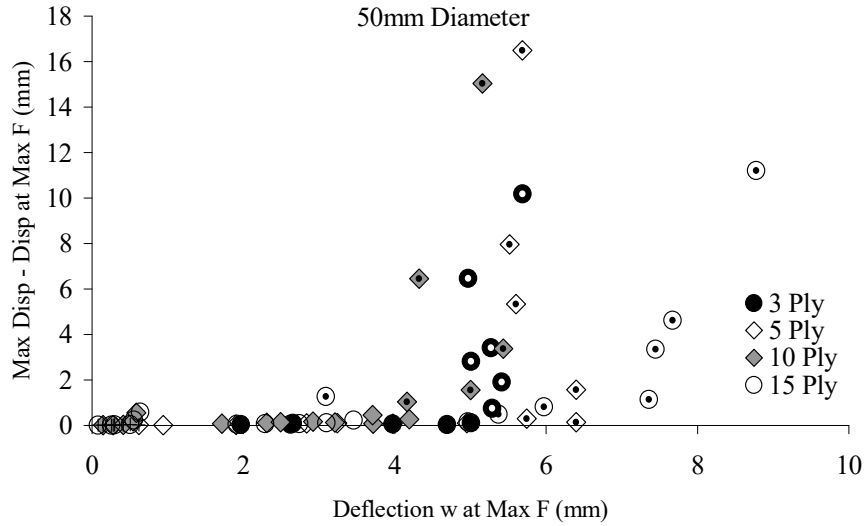

Fig. 19. Fibre damage parameter vs. deflection, small specimens.

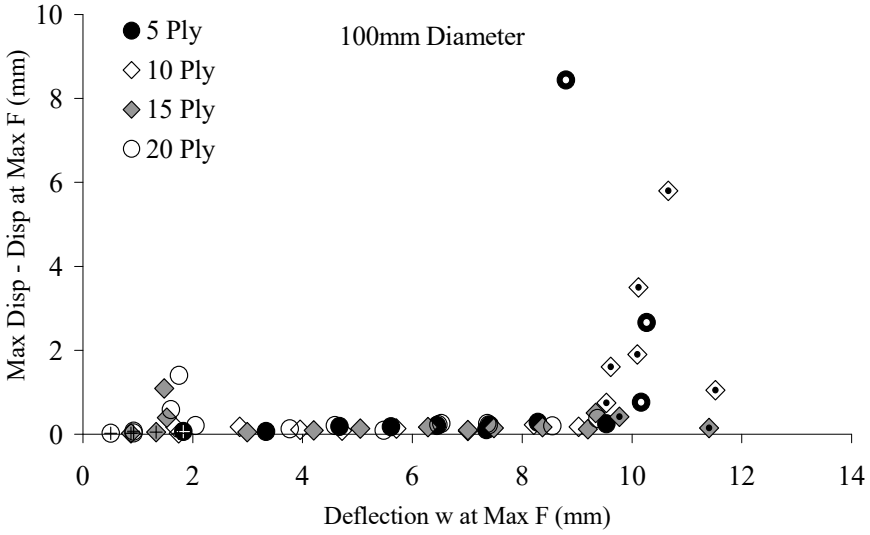

Fig. 20. Fibre damage parameter vs. deflection, large specimens.

The equivalent plots against force for the small specimens (Fig. 21) shows that fibre failure of the 15-ply laminates starts at approximately the same maximum force as for the 10-ply specimens. This provides some, but inconclusive, evidence of the onset of behaviour consistent with damage path (ii) for the thickest laminates.

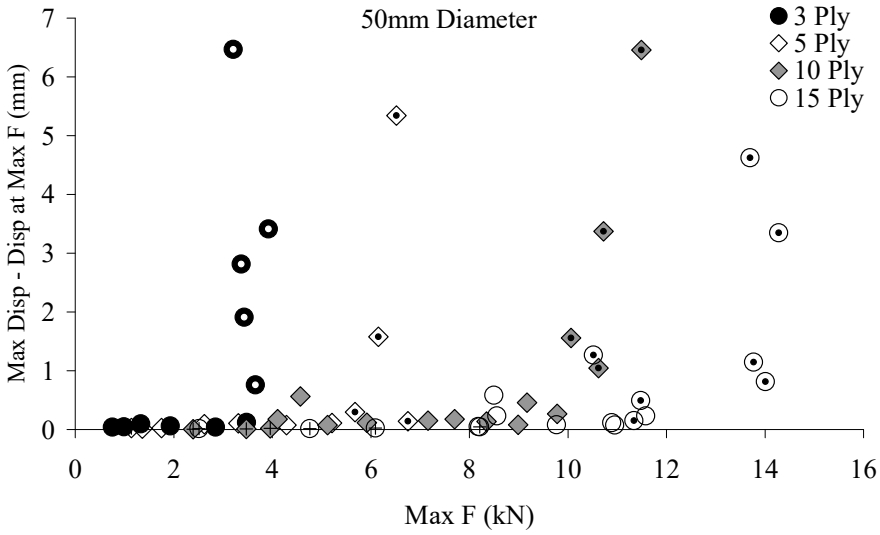

Fig. 21. Fibre damage parameter vs. maximum force, small specimens.

4.6. Damaged area

Delamination consisted of roughly circular areas at more than one laminate interfaces. Here, only the projected delaminated area is measured, and this is probably equal to the area of the largest delamination. This damage is thought to be shear driven, but is also influenced by the complex stress field around the contact area and the fairly coarse woven reinforcement architecture. Thus, the prediction of damage area is extremely complex, as well as completely dependent on complex and sensitive (to many material and testing variables) damage paths, and hence is beyond the scope of this paper. However, the theory of Section 4.2 suggests that plotting the damage against IKE normalised by laminate thickness, as in Figs. 22 and 23, would allow comparison of the damage at 'equivalent' IKE's for laminates of differing numbers of plies.

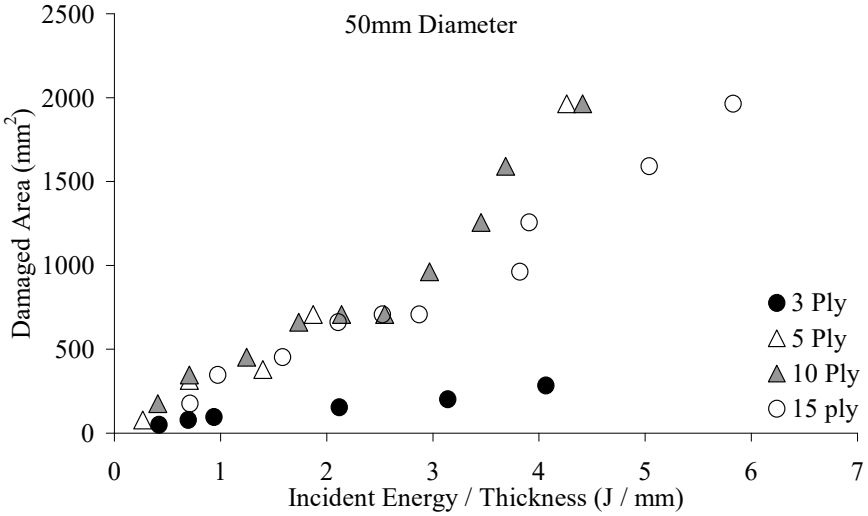

Fig. 22. Circular damage areas, small specimens.

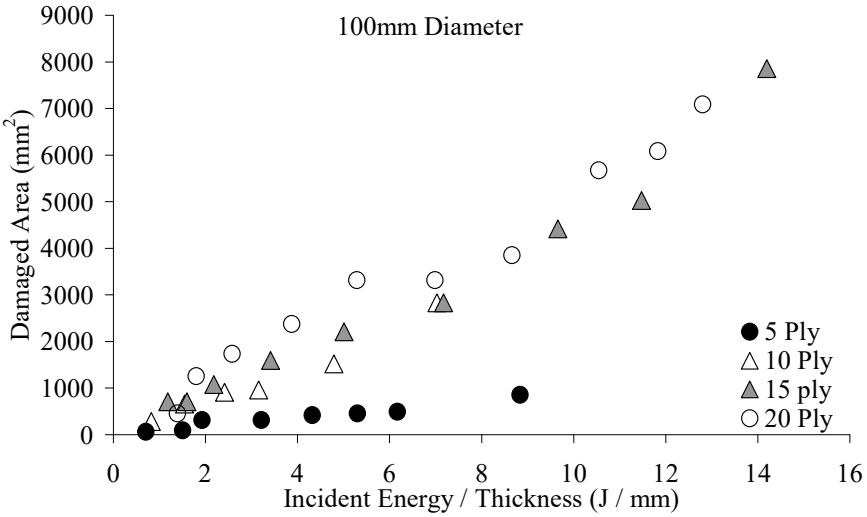

Fig. 23. Circular damage areas, large specimens.

Although some linear relationships between damaged area and IKE/*h* is seen, the behaviour is not clear-cut. Fig. 22 shows that the damage areas for the 5-, 10- and 15-ply small specimens collapse onto a fairly consistent trend followed by a 'plateau' up to an IKE/*h* value of about 3, but thereafter data diverges. Conversely, the slopes of the linear relationships corresponding to 10-, 15- and 20-ply laminates in Fig. 23 increase with laminate thickness up to a value of IKE/*h* of about 6, but above this value the data for the 15- and 20-ply specimens lie approximately on the same trend. What is clear is that the more flexible thinnest laminates for each specimen diameter have markedly less delamination than the other specimens for any given 'equivalent' IKE. This corresponds with the previous observation that although delamination occurred this was not seen to affect the response of the thinnest laminates.

5. Conclusions

Drop-weight impact tests have been carried out for low fibre-volume glass-polyester laminates for two geometrically scaled circular specimen sizes and for a range of diameter to thickness ratios.

The impact behaviour has been characterised as a progression of three damage stages with increasing incident energy, namely 'Un-delaminated', 'Delaminated' and 'Fibre damage'. A step-by-step inspection and analysis of the data then allowed characterisation of the complex impact response. A mainly graphical approach was taken, using deviations from a simplified mathematical model to identify the various controlling mechanisms. This methodology raised the following points for the impact behaviour of marine composites:

- Impact damage occurs in two stages: hidden internal delamination damage at low incident energy, and then finally perforation failure. Hence, high strain to failure reinforcement fibres will improve the perforation resistance, but good interlaminar shear properties are also required to delay and reduce delamination.
- Bending and membrane effects are significant for thin laminates. For thick laminates, especially after the sudden onset of delamination, the response is shear-dominated, and at higher incident energies significant indentation damage occurs.

- Even for barely visible damage a high proportion of the impact energy is irreversibly absorbed. It is not known whether this is due to damage or other mechanisms.
- Some form of effect of strain-rate on material response is thought to be significant when bending dominates (thinner plates), but this is not seen for the shear controlled deflections of thicker plates or when significant damage occurs.
- Indentation follows the Hertzian contact law at low contact forces, but a linear contact stiffness is seen at higher forces due to local delamination and fibre damage.
- A fracture mechanics model describes extremely well the sudden onset of delamination, and gives good scaling between specimen sizes.
- An energy balance approach gives good correlation between impact force and incident energy.
- Fibre failure leading to penetration is back-face tension controlled, although fibre shear-out may become important for very low diameter to thickness ratios.

The complex behaviour observed shows that the impact response must be characterised before mathematical modelling may be attempted. Any exact mathematical modelling of where damage is present must be correspondingly complex. Considering that any model assumptions concerning damage pathways will be easily invalidated (even by slight change in raw materials for example), that many of material properties required are unavailable and/or very difficult to measure accurately (if at all), and importantly that the exact micro-structure of marine composites is to some degree random, the practical use of such exact models for these materials is thought to be questionable. Modelling of the un-delaminated behaviour should consider bending, shear, indentation and membrane effects.

Acknowledgements

The first author has been financed by the Portuguese Foundation of Science and Technology under the contract number SFRH/BPD/1568/2000.

References

[1] Zhou G, Davies GAO. Impact response of thick glass fibre reinforced polyester laminates. Int J Impact Eng 1995;16(3):357-374.

[2] Mouritz AP, Gellert E, Burchill P and Challis K. Review of advanced composite structures for naval ships and submarines. Composite Structures 2001;53:21-41.

[3] Abrate S. Impact on composite structures. Cambridge University Press, 1998.

[4] Sun CT., Dicken A., Wu HF. Characterization of impact damage in ARALL laminates. Composite Science and Technology 1993;49:139-144.

[5] Tan TM. and Sun CT. Use of statical indentation laws in the impact analysis of laminated composite plates. Trans. ASME 1985;52:6-12.

[6] Chen JK. and Sun CT. Dynamic large deflection response of composite laminate subject to impact. Composite Structures 1985;4(1):59-73.

[7] Naik NK, Chandra Sekher Y and Sailendra Meduri. Damage in woven-fabric composites subjected to low-velocity impact. Composites Science and Technology 2000; 60:731-744.

[8] Richardson MOW. and Wisheart MJ. Review of low-velocity impact properties of composite materials. Composites Part A 1996;27A:1123-1131.

[9] Cartié DDR. and Irving PE. Effect of resin and fibre properties on impact and compression after impact performance of CFRP. Composites: Part A 2002;33:483-493.

[10] Caprino G. and Lopresto V. On the penetration energy for fibre-reinforced plastics under low-velocity impact conditions. Composite Science and Technology 2001;61:65-73.

[11] Hirai Y., Hamada H. and Kim JK. Impact response of woven glass-fabric composites – I. Effect of fibre surface treatment. Composite Science and Technology 1998;58:91-104.

[12] Abrate S. Modelling of impacts on composite structures. Composite Structures 2001; 51:129-138.

[13] Christoforou AP. Impact dynamics and damage in composite structures. Composite Structures 2001;52:181-188.

[14] Sutherland LS. and Guedes Soares C. The effects of test parameters on the impact response of glass reinforced plastic using an experimental design approach. Composites Science and Technology 2003;63:1-18.

[15] Caprino G., Langella A. and Lopresto V. Elastic behaviour of circular composite plates transversely loaded at the centre. Composites: Part A 2002;33:1191-1197.

[16] Caprino G., Langella A. and Lopresto V. Indentation and penetration of carbon fibre reinforced plastic laminates. Composites: Part B 2003;34:319-325.

[17] Berlingardi G. and Vadori R. Low velocity impact tests of laminate glass-fiber-epoxy matrix composite material plates. Int J Impact Eng 2002;27:213-229.

[18] Berlingardi G. and Vadori R. Influence of the laminate thickness in low velocity impact behavior of composite material plate. Composite Structures 2003;61:27-38

[19] Hancox, NL. and Mayer RM. Design Data for Reinforced Plastics. Chapman and Hall, 1993.

[20] Shivakumar KN., Elber W. and Illg W. Prediction of impact force and duration due to low-velocity impact on circular composite laminates. J. Appl. Mech. 1985;52:674-680.

[21] Timoshenko SP. and Woinowsky-Krieger S. Theory of plates and shells. Mcgraw-Hill, 1959.

[22] Sutherland LS. and Guedes Soares C. Effects of laminate thickness and reinforcement type on the impact behaviour of e-glass/polyester laminates. Composites Science and Technology 1999;59:2243-2260.

[23] Davies GAO. and Zhang X. Impact damage prediction in carbon composite structures. Int J Impact Eng 1995;16(1):149-170.

[24] Davies GAO., Hitchings D. and Zhou G. Impact damage and residual strengths of woven fabric glass/polyester laminates. Composites Part A 1993;27A:1147-1156.